Available online at www.sciencedirect.com
ScienceDirect
Ceramics International 38 (2012) 411–415
CERAMICS INTERNATIONAL
www.elsevier.com/locate/ceramint

Simple fabrication of polyhedral grain-like microparticle $Cu_{0.5}Zn_{0.5}HPO_4{\cdot}H_2O$ and porous structure $CuZnP_2O_7$

Banjong Boonchom [a,*], Naratip Vittayakorn [b,c,d]

[a] King Mongkut's Institute of Technology Ladkrabang, Chumphon Campus, 17/1M. 6 Pha Thiew District, Chumphon 86160, Thailand
[b] Electroceramic Research Laboratory, College of Nanotechnology, King Mongkut's Institute of Technology Ladkrabang, Bangkok 10520, Thailand
[c] Advanced Materials Science Research Unit, Department of Chemistry, Faculty of Science, King Mongkut's Institute of Technology Ladkrabang, Bangkok 10520, Thailand
[d] ThEP Center, CHE, 328 Si Ayutthaya Rd., Bangkok 10400, Thailand

Received 6 April 2011; received in revised form 3 July 2011; accepted 5 July 2011
Available online 20th July 2011

Abstract

Polyhedral grain-like microparticle $Cu_{0.5}Zn_{0.5}(HPO_4){\cdot}H_2O$ was simply synthesized by heterogeneous reaction using a mixture of $CuCO_3$, ZnO, phosphoric acid and water at room temperature for 30 min. The thermogravimetric study indicates that the synthesized compound is stable below 250 °C and its final decomposed product is $CuZnP_2O_7$. The pure monoclinic phases of the synthesized $Cu_{0.5}Zn_{0.5}(HPO_4){\cdot}H_2O$ and its final decomposed product $CuZnP_2O_7$ are verified by XRD data. The presences of the HPO_4^{2-} ion and H_2O molecule in the $Cu_{0.5}Zn_{0.5}(HPO_4){\cdot}H_2O$ structure and the $P_2O_7^{4-}$ ion in the $CuZnP_2O_7$ structure are confirmed by FTIR data. The thermal stability, the morphology based on polyhedral grain-like microparticles and porous structure of the studied compounds are different from previously reported phosphates, and may affect their activities for potential applications (catalysis, electronics, etc.).

Keywords: Polyhedral grain-like particle; Ceramic pigment; Thermal behaviors; Metal phosphates; Powder synthesis

1. Introduction

Metal phosphates may be classified by its phosphate block units (PO_4^{3-}, HPO_4^{2-}, $H_2PO_4^{-}$, $P_2O_7^{4-}$ and $P_4O_{12}^{4-}$) and attract increasing interest for environmental and technological fields [1]. In environmental field, the formation of metal phosphates help remove phosphate from waste waters, while their dissociations help regulate the slow release of fertilizers (P-macronutrient and metal-micronutrients) in acidic soils [2]. In technological field, the interest of metal phosphates is mainly focused on areas such as laser host [3], ceramic [4], dielectric [5], electric [5], magnetic [6], fertilizer [7], and catalytic [8] processes because of their valuable physical–chemical properties and reactivities. Consequently, metal phosphates have become a hot research topic in academic (material and chemical sciences) and industrial fields in the recent years [9–11].

One metal phosphate group, corresponding to the formula $M(HPO_4){\cdot}nH_2O$ (M = Mg, Ca, Mn, Co, Cu, Ni and Zn, $0 < n < 3$)[12–17], is a promising candidate for application in the fields of catalysis, electrics, ion exchange and conductors [3–8]. Because of their acidity and porosity, layered materials represent a vast class of intercalating compounds with useful chemical and thermal properties, which have been extensively used as heterogeneous catalysts [8,18]. Furthermore, thermal treatment of this metal hydrogen phosphate group has a great synthetic potential as it may turn simple compounds into advanced materials, which occur through hydrolysis and dehydration reactions at high temperatures [12–17]. Their final decomposed products belong to the metal pyrophosphate group ($M_2P_2O_7$; M = Mg, Mn, Co, Ni, Cu and Zn), which can be used for wide applications according to above mentioned [1–8]. More recently, many works have been directed towards the synthesis of binary metal hydrogen phosphates ($M_{1-x}A_x(HPO_4){\cdot}nH_2O$ and metal pyrophosphates ($M_{2-y}A_yP_2O_7$) (M or A = Mg, Ca, Mn, Co, Cu, Ni and Zn, $0 < n < 3$; $0 < x < 1$; $0 < y < 2$) [19–21]. Accordingly, it is pertinent to prepare $M_{1-x}A_x(HPO_4){\cdot}nH_2O$, $M_{2-y}A_yP_2O_7$ and their solid solutions, since they may offer some

* Corresponding author. Tel.: +66 7750 6422×4565; fax: +66 7750 6411.
E-mail address: kbbanjon@gmail.com (B. Boonchom).

0272-8842/$36.00
doi:10.1016/j.ceramint.2011.07.022

excellent physical and chemical properties when the composition is varied. So far, copper zinc hydrogen phosphate has not been reported in the literature. However, copper and zinc have received a great deal of attention due to its friendly environmental character and the associated low costs.

The attempt of this work is to prepare $Cu_{0.5}Zn_{0.5}(HPO_4)\cdot H_2O$ powder by heterogeneous reaction using copper carbonate, zinc oxide, phosphoric acid and water at room temperature for 30 min. Additionally, the $CuZnP_2O_7$ powder has been also obtained from calcination of $Cu_{0.5}Zn_{0.5}(HPO_4)\cdot H_2O$ at 300 °C for 3 h in air atmosphere. This method is a simple, cost- and time-saving route to synthesize $Cu_{0.5}Zn_{0.5}(HPO_4)\cdot H_2O$ and $CuZnP_2O_7$. The studied powders were characterized by thermogravimetry–differential thermogravimetry (TG/DTG), differential scanning calorimetry (DSC), X-ray diffraction (XRD), Fourier transform infrared (FTIR) and scanning electron microscope (SEM) techniques. The data obtained will be important for further studies of the compound.

2. Experimental

The binary $Cu_{0.5}Zn_{0.5}(HPO_4)\cdot H_2O$ compound was prepared by heterogeneous reaction using $CuCO_3$ (99.99%, Merck), ZnO (99.99%, Merck) and H_3PO_4 (86.4%,w/w Merck) as starting materials. Following procedure, 10 mL of acetone were added to mixed solids of 1.24 g of $CuCO_3$ and 0.82 g of ZnO (corresponding to a nominal Mn:Co molar ratio of 1:1) and this suspension was referred to as mixture A. Then, 5 mL of 70% H_3PO_4 (82.02 mL of 86.4%,w/w H_3PO_4 dissolved in 18.98 mL of DI water) was added to the mixture A. The resulting suspension was continuously stirred at room temperature until CO_2(g) was completely evolved and the precipitates were obtained within about 15 min. This process can be explained by the following reaction

$$\frac{1}{2}CuCO_3(s) + \frac{1}{2}ZnO(s) + H_3PO_4(aq) \xrightarrow{\text{acetone, room temperature}} Cu_{0.5}Zn_{0.5}(HPO_4)\cdot H_2O(s) + \frac{1}{2}CO_2(g)$$

The pale blue solid of $Cu_{0.5}Zn_{0.5}HPO_4\cdot H_2O$ product was filtered by suction pump, washed with acetone until free from phosphate ion, dried in air and then kept in desiccator. The water content of the sample was determined by TG data, which reveals the completely decomposed product at temperatures above 250 °C. The dried pale blue solid then was calcined in a box-furnace at 300 °C for 3 h in air and a final decomposed product $CuZnP_2O_7$ was obtained.

The metal contents of the synthesized $Cu_{0.5}Zn_{0.5}H_2PO_4\cdot H_2O$ and its decomposed product $CuZnP_2O_7$ were determined by atomic absorption spectrophotometry (AAS, Perkin Elmer, Analyst100) after dissolution in 0.0126 M hydrochloric acid. The phosphorus content was determined by colorimetric analysis of the molybdophosphate complex. Thermal transformation of the synthesized $Cu_{0.5}Zn_{0.5}H_2PO_4\cdot H_2O$ was investigated on a Pyris Diamond TG/DTG Perkin Elmer Instrument and a Diamond DSC Perkin-Elmer apparatus. The experiments were carried out in air atmosphere by increasing temperature at heating rates of 10 °C min^{-1} from 30 to 550 °C with α-Al_2O_3 as the reference material. The room temperature FTIR spectra were recorded in the range of 4000–370 cm^{-1} with eight scans on a Perkin Elmer Spectrum GX FT-IR spectrometer with the resolution of 4 cm^{-1} using KBr pellets (spectroscopy grade, Merck). The structures and crystallite sizes of the prepared product and its decomposed product were studied by X-ray powder diffraction using a D8 Advanced powder diffractometer (Bruker AXS, Karlsruhe, Germany) with Cu Kα radiation (λ = 0.1546 nm). The Scherrer method was used to evaluate the crystallite size (i.e. $D = K\lambda/\beta\cos\theta$, where λ is the wavelength of X-ray radiation, K is a constant taken as 0.89, θ is the diffraction angle and β is the full width at half maximum (FWHM)) [22]. The morphologies of the selected resulting samples were examined by scanning electron microscope (SEM) using LEO SEM VP1450 after gold coating.

3. Results and discussion

The TG/DTG curves of $Cu_{0.5}Zn_{0.5}HPO_4\cdot H_2O$ are shown in Fig. 1. The TG curve of $Cu_{0.5}Zn_{0.5}HPO_4\cdot H_2O$ shows the two weight loss steps in the range of 50–550 °C. The weight loss steps in the TG curve were observed in ranges of 50–150 and 150–400 °C. The corresponding observed weight losses were 4.69 and 14.79% by mass, which correspond to 0.5 and 1.47 mol of water, respectively. The first stage of the weight loss was related to the loss of moisture because it is not stable over 100 °C. While the second stage was due to the loss of water molecules from overlapping reactions: the loss of coordination water (dehydration reaction) and the deprotonation of hydrogen phosphate groups (condensation reaction). These two stages appear in the corresponding DTG and DSC curves as two peaks (55 and 178 °C). The retained mass of about 80.52% is compatible with the value expected for the formation of $CuZnP_2O_7$, which is confirmed by XRD and FTIR data. The thermal decomposition of the studied $Cu_{0.5}Zn_{0.5}H_2PO_4\cdot H_2O$ involves the dehydration of the coordinated water molecule and an intramolecular dehydration (condensation) of

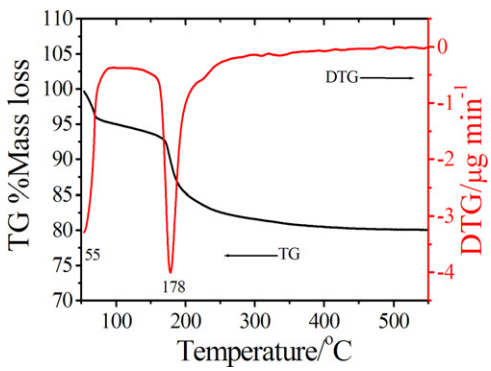

Fig. 1. TG/DTG curves of the synthesized $Cu_{0.5}Zn_{0.5}HPO_4\cdot H_2O$ at the heating range of 10 °C min^{-1}.

the protonated phosphate groups. These processes formally could be presented as:

$$Cu_{0.5}Zn_{0.5}HPO_4{\cdot}1.5H_2O \rightarrow Cu_{0.5}Zn_{0.5}HPO_4{\cdot}H_2O + \sim 0.5H_2O \quad (1)$$

$$Cu_{0.5}Zn_{0.5}HPO_4{\cdot}H_2O \rightarrow 1/2CuZnP_2O_7 + 1.5H_2O \quad (2)$$

The final product of the thermal decomposition at $T > 400$ °C is found to be a binary copper zinc pyrophosphate, $CuZnP_2O_7$. For hydrate content analysis, the observed total mass loss of 14.79% (1.47 mol H_2O) is close to theoretical value of 15.13% (1.50 mol H_2O). The thermal behaviors (thermal stability, mechanism and phase transition temperature) of $Cu_{0.5}Zn_{0.5}HPO_4{\cdot}H_2O$ differ from those of the individual compounds ($CuHPO_4{\cdot}H_2O$ [15] and $ZnHPO_4{\cdot}H_2O$ [17]), which are caused by the homogeneous incorporation of Cu and Zn metals in the skeleton. The formations of new binary $Cu_{0.5}Zn_{0.5}HPO_4{\cdot}H_2O$ and its decomposed product $CuZnP_2O_7$ confirmed by XRD and FTIR data agree with this thermal analysis result. Thus, in this work we have obtained a $CuZnP_2O_7$ powder through a simple, rapid, cost-saving route, in comparison to previous synthesis of other metal pyrophosphates, $M_2P_2O_7$ (M = Mn, Co, Cu, Zn, Ni) [12–17].

The DSC curve of $Cu_{0.5}Zn_{0.5}HPO_4{\cdot}H_2O$ in N_2 is shown in Fig. 2. The DSC trace shows two endothermic peaks at 85 and 177 °C (onset peak at 40 and 130 °C) which are due to the moisture loss and the overlapping reactions between dehydration and deprotonated hydrogenphosphate, respectively. According to the DSC curve, the heat of two thermal transformation steps can be calculated and were found to be 52.74 and 258.47 J g^{-1}, respectively. The obtained DSC result is consistent with TG/DTG data (Fig. 1).

The XRD pattern of $Cu_{0.5}Zn_{0.5}HPO_4{\cdot}H_2O$ is similar to that of $CuHPO_4{\cdot}H_2O$ (monoclinic phase), which is significantly different from that of $ZnHPO_4{\cdot}mH_2O$ (orthorhombic phase; $m = 1, 3$) while the XRD pattern of its decomposed product $CuZnP_2O_7$ is similar to those of β-$Zn_2P_2O_7$ and β-$CuZnP_2O_7$ (monoclinic phases) (Fig. 3). This indicates that the synthesized $Cu_{0.5}Zn_{0.5}HPO_4{\cdot}H_2O$ and $CuZnP_2O_7$ show dominant characteristic of monoclinic phase based on the $CuHPO_4{\cdot}H_2O$ structure and β-$Zn_2P_2O_7$ form, respectively. On the basis of the XRD analysis, the quite similar XRD patterns between the systems of binary metal solid solution and single metal solid are caused by the equivalent electric charges and the close radii of cations, which support that they are isostructural [19–21]. Consequently, we can draw a conclusion that the synthesized

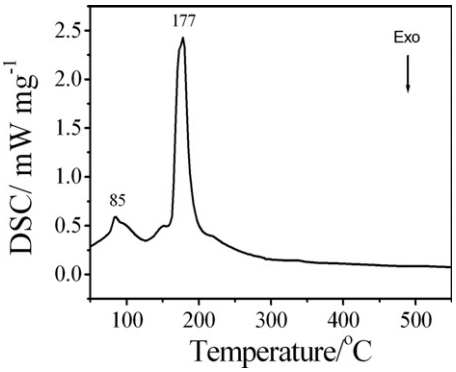

Fig. 2. DSC curve of the synthesized $Cu_{0.5}Zn_{0.5}HPO_4{\cdot}H_2O$ at the heating range of 10 °C min^{-1}.

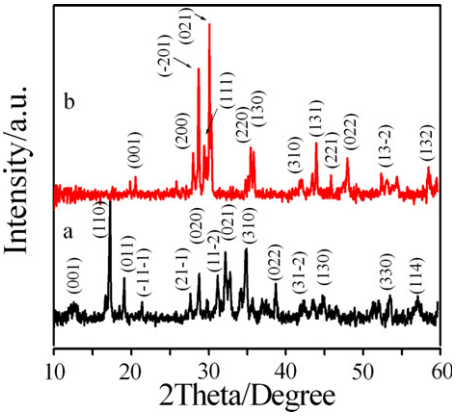

Fig. 3. XRD patterns of the synthesized $Cu_{0.5}Zn_{0.5}HPO_4{\cdot}H_2O$ (a) and its decomposed product $CuZnP_2O_7$ (b).

$Cu_{0.5}Zn_{0.5}HPO_4{\cdot}H_2O$ and $CuZnP_2O_7$ are solid solutions and not a mixture of single phase of the individual ones. Hence, the obtained XRD patterns were compared with the standard XRD patterns of $CuHPO_4{\cdot}H_2O$ (PDF no. 83-1857 for Cu), β-$Zn_2P_2O_7$ (PDF no. 34-1275) and β-$CuZnP_2O_7$ (PDF no. 82-0973), respectively (Fig. 3). All reflections can be distinctly indexed based on pure monoclinic phases with space group $P2_1/a$ ($Z = 4$) for $Cu_{0.5}Zn_{0.5}HPO_4{\cdot}H_2O$ and space group C2/m ($Z = 4$) for β-$CuZnP_2O_7$, which noted to be similar to those of the standard XRD patterns of $CuHPO_4{\cdot}H_2O$ (PDF no. 83-1857), β-$Zn_2P_2O_7$ (PDF no.34-1275) and β-$CuZnP_2O_7$ (PDF no. 82-0973), respectively. The average crystallite sizes and lattice parameters of $Cu_{0.5}Zn_{0.5}HPO_4{\cdot}H_2O$ and $CuZnP_2O_7$ samples were calculated from XRD patterns and tabulated in Table 1. The lattice parameters of $Cu_{0.5}Zn_{0.5}HPO_4{\cdot}H_2O$ and $CuZnP_2O_7$ are comparable to those of the standard data.

Table 1
Average crystallite size and lattice parameter of $Cu_{1/2}Zn_{1/2}HPO_4{\cdot}H_2O$ and $CuZnP_2O_7$ calculated from XRD data.

Compound	Method	a (Å)	b (Å)	c (Å)	β (?)	Average crystallite size (nm)
$CuHPO_4{\cdot}H_2O$	PDF no. 83-1857	8.61	6.35	6.81	94.16	
$Cu_{1/2}Zn_{1/2}HPO_4{\cdot}H_2O$	This work	8.74(2)	6.32(1)	6.80(0)	93.98(1)	42 ± 11
$ZnHPO_4{\cdot}3H_2O$	PDF no. 39-0439	10.98	8.46	25.69	–	
β-$CuZnP_2O_7$	This work	6.81(2)	8.14(0)	4.53(2)	106.46(3)	65 ± 20
β-$CuZnP_2O_7$	PDF no. 82-0973	6.74	8.19	4.54	107.72	
β-$Zn_2P_2O_7$	PDF no. 34-1275	6.61	8.29	4.51	105.40	

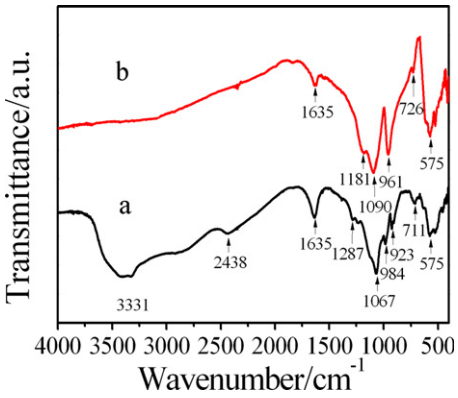

Fig. 4. FTIR spectra of the synthesized $Cu_{0.5}Zn_{0.5}HPO_4{\cdot}H_2O$ (a) and its decomposed product $CuZnP_2O_7$ (b).

The FTIR spectra of the synthesized $Cu_{0.5}Zn_{0.5}HPO_4{\cdot}H_2O$ and $CuZnP_2O_7$ powders (Fig. 4) assigned according to the literatures [23–25] reflect characteristic vibrations of HPO_4^{2-} anion and H_2O molecules and $P_2O_7^{4-}$ anion, respectively. Vibrational bands of HPO_4^{-2} ion are observed in the regions of 300–500, 700–900, 1067–1287, 840–984, 1000–1200, 2300–2438, 2800–3120, and 3200–3500 cm^{-1}. These bands are assigned to the $\delta(PO_3)$, $\gamma(POH)$, $\delta(POH)$, $\nu(PO_2(OH))$, $\nu(PO_3)$, B band (ν_{OH} HPO_4^{-2}), A band (ν_{OH} HPO_4^{-2}) and ν_{OH} (ν_1 and ν_3 H_2O), respectively. The observed center bands at 1635 cm^{-1} and 3331 cm^{-1} are assigned to water bending or band C and asymmetry O–H stretching (H_2O), respectively implying the presence of crystalline hydrate. For characteristic vibration of $CuZnP_2O_7$, FTIR bands are assigned according to the literature [24,25] based on the fundamental vibrating unit $P_2O_7^{4-}$ anion. One of the most noteworthy features of the spectrum is the presence of the strong bands at 1181, 1096, 961, 726, 575 and 526 cm^{-1}. These bands can be assigned to $\nu_{as}(PO_3)$, $\nu_{as}(POP)$, $\nu_s(POP)$, $\delta(PO_3)$, $\delta(PO_3)$, and $\rho(PO_3)$, respectively. The observed band 1635 cm^{-1} (Fig. 4b) assigned to water vibrations come from moisture absorption of KBr pellet.

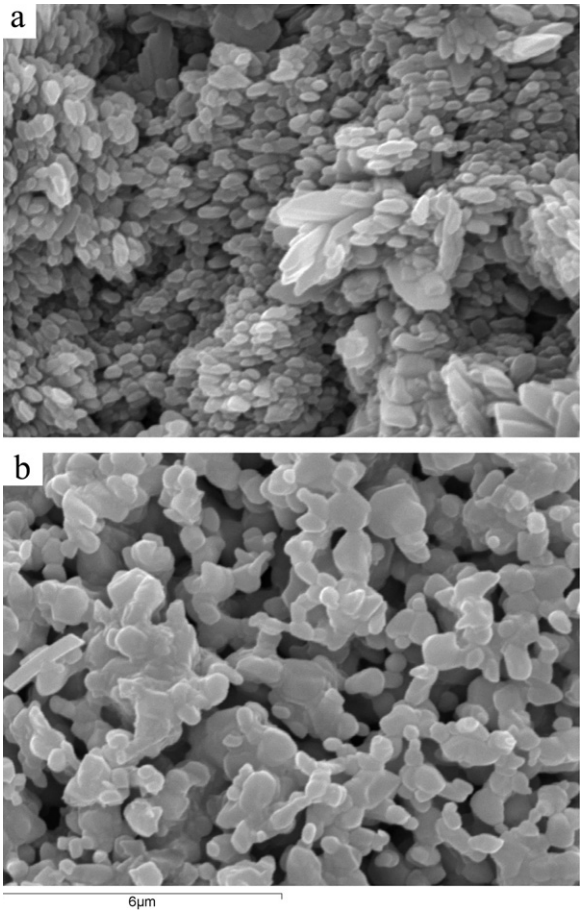

Fig. 5. SEM micrographs of the synthesized $Cu_{0.5}Zn_{0.5}HPO_4{\cdot}H_2O$ (a) and its decomposed product $CuZnP_2O_7$ (b).

The morphologies of $Cu_{0.5}Zn_{0.5}HPO_4{\cdot}H_2O$ and its decomposed product $CuZnP_2O_7$ powders are shown in Fig. 5. The $Cu_{0.5}Zn_{0.5}HPO_4{\cdot}H_2O$ powder prepared in this work shows polyhedral grain-like microparticles, which are not similar to those of other metal phosphates reported in previous works [13,19–21]. The polyhedral grain-like morphologies contain layers of small and large particles with porous structure while its decomposed product $CuZnP_2O_7$ shows a structure containing many of large pores, which is possibly caused by the dehydration and deprotonated hydrogen phosphate reactions. The morphologies of the synthesized $Cu_{0.5}Zn_{0.5}HPO_4{\cdot}H_2O$ and its decomposed product $CuZnP_2O_7$ in this work are significantly different from those of other phosphate compounds [13,19–21]. The porous structures may affect their performance as ceramic pigments, coatings or catalysts, which may be used for further works [26–28].

4. Conclusion

Polyhedral grain-like microparticle $Cu_{0.5}Zn_{0.5}HPO_4{\cdot}H_2O$ was successfully synthesized by heterogeneous reaction using the mixture of $CuCO_3$, ZnO, phosphoric acid and water at room temperature for 30 min. The $Cu_{0.5}Zn_{0.5}HPO_4{\cdot}H_2O$ transforms to $CuZnP_2O_7$ via two overlapping reactions of dehydration and the deprotonation (condensation) of the hydrogen phosphate groups. In this work we have reported the synthesis of $CuZnP_2O_7$ pyrophosphate through an easy, cost- and time-saving route, in comparison with previous synthesis of other metal pyrophosphates. The XRD and FTIR results confirmed the formation of $Cu_{0.5}Zn_{0.5}HPO_4{\cdot}H_2O$ and its decomposed product $CuZnP_2O_7$. The thermal behaviors, polyhedral grain shapes, porous structures, particle size and crystallite sizes of the synthesized $Cu_{0.5}Zn_{0.5}HPO_4{\cdot}H_2O$ and $CuZnP_2O_7$ are reported for the first time and differed from previous reports. The results obtained are necessary for theoretical study, applications development, and industrial production of binary metal hydrogen phosphate hydrates and metal pyrophosphates, which may have interesting and potential applications for further works.

Acknowledgments

Thai work financially supported by KMITL Research Fund and the National Nanotechnology Center (NANOTEC) NSTDA, Ministry of Science and Technology, Thailand.

References

[1] M.T. Averbuch-Pouchot, A. Durif, Topics in Phosphate Chemistry, World Scientific Publishing Co. Pte. Ltd., Singapore, 1996.

[2] A. Silber, B. Bar-Yosef, I. Levkovitch, L. Kautzky, D. Minz, Kinetics and mechanism of pH-dependent Mn(II) reactions in plant-growth medium, Soil Biology and Biochemistry 401 (2008) 2787–2795.

[3] A. Jouini, J.C. Gâcon, M. Ferid, M. Trabelsi-Ayadi, Luminescence and scintillation properties of praseodymium poly and diphosphates, Optic Materials 24 (2003) 175–180.

[4] H.-I. Hsiang, L.-T. Mei, Y.-H. Lin, Formation and growth of manganese phosphate passivation layers for NTC ceramics, Journal of Alloys Compounds 48 (2009) 723–728.

[5] L. Adam, A. Guesdon, B. Raveau, Unique charge ordering of manganese in a new mixed valent phosphate $K_3Mn_3^{II}Mn^{III}(PO_4)(H_{0.5}PO_4)_2(HPO_4)_2$, Journal of Solid State Chemistry 182 (2009) 2338–2343.

[6] D. Feng, C. Wang, W. Cheng, G. Li, S. Tian, F. Liao, M. Xiong, J. Lin, Synthesis, crystal structure, and magnetic properties of $K_4Mn_3(HPO_4)_4(H_2PO_4)_2$, Solid State Sciences 11 (2009) 845–851.

[7] A. Yuan, L. Wu, S. Bai, Z. Ma, Z. Huang Tong, Standard molar enthalpies of formation for ammonium/3d-transition metal phosphates $NH_4MPO_4{\cdot}H_2O$ ($M = Mn^{2+}$, Co^{2+}, Ni^{2+}, Cu^{2+}), Journal of Chemistry and Engineering Data 53 (2008) 1066–1070.

[8] B.Y. Jibril, S.M. Al-Zahrani, A.E. Abasaeed, Propane oxidative dehydrogenation over metal pyrophosphates catalysts, Catalysis Letters 74 (2001) 145–148.

[9] B. Boonchom, R. Baitahe, Z. Joungmunkong, N. Vittayakorn, Grass blade-like microparticles $MnPO_4{\cdot}H_2O$ prepared by a simple precipitation at room temperature, Powder Technology 203 (2010) 310–314.

[10] G. Qiu, Z. Gao, H. Yin, X. Feng, W. Tan, F. Liu, Synthesis of $MnPO_4{\cdot}H_2O$ by refluxing process at atmospheric pressure, Solid State Sciences 12 (2010) 808–813.

[11] S. Ping Ong, A. Jain, G. Hautier, B. Kang, G. Ceder, Thermal stabilities of delithiated olivine MPO_4 (M = Fe, Mn) cathodes investigated using first principles calculations, Electrochemistry Communications 12 (2010) 427–430.

[12] B. Boonchom, Kinetic and thermodynamic studies of $MgHPO_4{\cdot}3H_2O$ by non-isothermal decomposition data, Journal of Thermal Analysis and Calorimetry 98 (2009) 863–871.

[13] B. Boonchom, C. Danvirutai, A simple synthesis and thermal decomposition kinetics of $MnHPO_4{\cdot}H_2O$ rod-like microparticles obtained by spontaneous precipitation route, Journal of Optoelectronics and Advance Materials 10 (2008) 492–499.

[14] D. Brandová, M. Trojan, M. Arnold, F. Paulik, J. Paulik, Mechanism of the dehydration of $CoHPO_4{\cdot}1.5H_2O$, Journal of Thermal Analysis 34 (1988) 673–678.

[15] D. Brandová, M. Trojan, M. Arnold, F. Paulik, J. Paulik, Mechanism of the dehydration of $CuHPO_4{\cdot}H_2O$, Journal of Thermal Analysis 34 (1988) 1449–1454.

[16] S. Rosa, H.E. Lundager Madsen, Influence of some foreign metal ions on crystal kinetics of brushite $CaHPO_4{\cdot}2H_2O$, Journal of Crystal Growth 45 (2010) 2983–2988.

[17] D. Brandová, M. Trojan, F. Paulik, J. Paulik, Mechanism of the dehydration of $ZnHPO_4{\cdot}H_2O$, Journal of Thermal Analysis 32 (1987) 1923–1928.

[18] M.A. Aramendía, V. Borau, C. Jiménez, J.M. Marinas, F.J. Romero, Synthesis and characterization of magnesium phosphates and their catalytic properties in the conversion of 2-hexanol, Journal of Colloid Interface Sciences 217 (1999) 288–298.

[19] B. Boonchom, C. Danvirutai, Synthesis of $MnNiP_2O_7$ and nonisothermal decomposition kinetics of a new binary $Mn_{0.5}Ni_{0.5}HPO_4{\cdot}H_2O$ precursor obtained from a rapid coprecipitation at ambient temperature, Industrial Engineering and Chemistry Research 47 (2008) 5976–5981.

[20] B. Boonchom, N. Phuvongpha, Synthesis of new binary cobalt iron pyrophosphate $CoFeP_2O_7$, Materials Letters 63 (2009) 1709–1711.

[21] B. Boonchom, N. Vittayakorn, Synthesis and ferromagnetic property of new binary copper iron pyrophosphate $CuFeP_2O_7$, Materials Letters 63 (2010) 275–277.

[22] B.D. Cullity, Elements of X-ray Diffraction, second ed., Addison-Wesley Publishing, 1977.

[23] B. Ŝoptrajanova, B.V. Stefava, I. Kuzmanovskia, G. Jovanovskia, Fourier transform infrared and Raman spectra of manganese hydrogen phosphate trihydrate, Journal of Molecular Structure 103 (1999) 103–107.

[24] N.B. Colthup, L.H. Daly, S.E. Wiberley, Introduction to Infrared and Raman Spectroscopy, Academic Press, New York, 1964.

[25] E. Steger, B. Käßner, Die infrarotspektren von wasserfreien schwermetall-Diphosphaten, Spectrochimica Acta 24A (1968) 447–456.

[26] M. Llusar, J.A. Badenes, A. García, C. Gargori, R. Galindo, G. Monrós, Solid solutions of mixed metal $Mn_{3-x}Mg_xFe_4(PO_4)_6$ orthophosphates: colouring performance within a double-firing ceramic glaze, Ceramics International 37 (2) (2011) 493–504.

[27] S. Meseguer, M.A. Tena, C. Gargori, R. Galindo, J.A. Badenes, M. Llusar, G. Monrós, Development of blue ceramic dyes from cobalt phosphates, Ceramics International 34 (60) (2008) 1431–1438.

[28] M. Llusar, A. Zielinska, M.A. Tena, J.A. Badenes, G. Monrós, Blue-violet ceramic pigments based on Co and $MgCo_{2-x}Mg_xP_2O_7$ diphosphates, Journal of the European Ceramic Society 30 (9) (2010) 1887–1896.